

Chapter 2

Orientation Effects in Single-Domain Single Crystals

2.1 Single-Domain $0.67\text{Pb}(\text{Mg}_{1/3}\text{Nb}_{2/3})\text{O}_3 - 0.33\text{PbTiO}_3$

Full sets of electromechanical constants of perovskite-type relaxor-ferroelectrics of solid solutions of PMN- x PT and PZN- x PT are often measured on polydomain or domain-engineered SC samples (see for instance, Refs. [1–6]). The full set of room-temperature electromechanical constants related to the single-domain state was first measured [7] on PMN-0.33PT SCs. This particular composition is very close to the MPB [8], and single-domain SCs at $x = 0.33$ are characterised by rhombohedral 3 m symmetry [9]. Based on experimental data [7] of the single-domain PMN-0.33PT SC, their piezoelectric coefficients d_{3j} ($j = 1$ and 3) [9, 10], dielectric permittivity ε_{33}^σ and ECF k_{33} [9] were calculated along arbitrary directions of the crystallographic axes, and also the spontaneous polarisation vector \mathbf{P}_s . The further study and generalisation of the orientation dependences of the electromechanical properties of the single-domain PMN-0.33PT SCs has been carried out in work [11].

Now we consider some features of the orientation dependences of the piezoelectric coefficients and ECFs of the aforementioned SC. It is assumed that the spontaneous polarisation vector \mathbf{P}_s of the single-domain sample is parallel to the $[001]_{rh}$ direction (Fig. 2.1a) and is connected with the rectangular co-ordinate system $(X_1 X_2 X_3)$ of the SC sample, where subscript “ rh ” denotes “rhombohedral”. The $[001]_{rh}$ direction coincides with the $[111]_c$ direction in the cubic (perovskite) unit cell, $O X_3 || [111]_c$, and the subscript “ c ” denotes “cubic”. An arbitrary SC orientation due to the transformation of the co-ordinate axes $(X_1 X_2 X_3) \rightarrow (X'_1 X'_2 X'_3)$ (Fig. 2.1b) is described in terms of the well-known Euler angles φ , ψ and θ [12]. Taking into account this transformation, we represent the electromechanical constants of the SC sample in $(X'_1 X'_2 X'_3)$ as tensor components

$$\varepsilon_{mn}^{\sigma'} = r_{mp} r_{nq} \varepsilon_{pq}^\sigma, \quad d'_{efg} = r_{ej} r_{fk} r_{gl} d_{jkl} \quad \text{and} \quad s_{rtuv}^{E'} = r_{ra} r_{tb} r_{uc} r_{vd} s_{abcd}^E. \quad (2.1)$$

In (2.1) the terms ε_{pq}^σ , d_{jkl} and s_{abcd}^E are tensor components of dielectric permittivities (second rank), piezoelectric coefficients (third rank) and elastic compliances

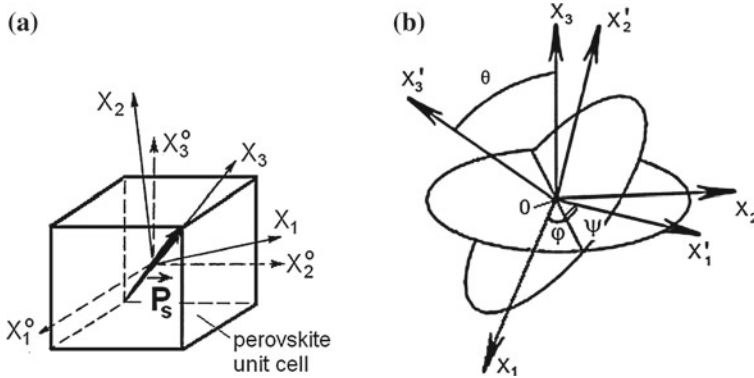


Fig. 2.1 Orientation of the domain with respect to the main crystallographic axes OX_j and perovskite unit-cell axes OX_j^o **a** and interconnections between the axes of co-ordinate systems $(X_1 X_2 X_3)$ and $(X'_1 X'_2 X'_3)$ **b**. P_s is the spontaneous polarisation vector in the rhombohedral phase, φ , ψ and θ are Euler angles

(fourth rank), respectively, and r_{mp} are elements of the rotation matrix

$$\|r\| = \begin{pmatrix} \cos \psi \cos \varphi - \sin \psi \cos \theta \cos \varphi & \cos \psi \sin \varphi + \sin \psi \cos \theta \cos \varphi & \sin \psi \sin \theta \\ -\sin \psi \cos \varphi - \cos \psi \cos \theta \sin \varphi & -\sin \psi \sin \varphi + \cos \psi \cos \theta \sin \varphi & \cos \psi \sin \theta \\ \sin \theta \sin \varphi & -\sin \theta \cos \varphi & \cos \theta \end{pmatrix}$$

that depends [12] on the above-mentioned Euler angles. We also highlight that a summation over the repeated subscripts [for instance, p and q in the $\varepsilon_{mn}^{\sigma'}$ formula from (2.1)] is performed from 1 to 3 in accordance with the Einstein summation notation at operations over tensor components.

After the transformation $(X_1 X_2 X_3) \rightarrow (X'_1 X'_2 X'_3)$ in accordance with (2.1), we use the conventional two-index form [12–15] for the notation of the electromechanical constants as written, for example, in Table 2.1. Based on the electromechanical constants from (2.1), it is possible to determine the orientation dependences of the

Table 2.1 Room-temperature elastic compliances s_{ab}^E (in 10^{-12}Pa^{-1}), piezoelectric coefficients d_{ij} (in pC/N) and dielectric permittivities $\varepsilon_{pp}^{\sigma}$ of the single-domain PMN–0.33PT SC (3m symmetry). Data from experimental work [7] ([9] in parentheses) are related to the main crystallographic axes OX_j shown in Fig. 2.1a

s_{11}^E	s_{12}^E	s_{13}^E	s_{14}^E	s_{33}^E	s_{44}^E	s_{66}^E
62.16	−53.85	−5.58	−166.24	13.34	510.98	232.02
(62.2)	(−53.8)	(−5.6)	(−166.2)	(13.3)	(511.0)	(232.0)
	d_{15}	d_{22}	d_{31}	d_{33}	$\varepsilon_{11}^{\sigma} / \varepsilon_0$	$\varepsilon_{33}^{\sigma} / \varepsilon_0$
	4,100	1,340	−90	190	3,950	640

remaining piezoelectric coefficients (g'_{ij} , e'_{ij} and h'_{ij}), ECFs k'_{ij} ¹ etc. Examples of the orientation dependences of the piezoelectric coefficients and ECFs of the single-domain PMN–0.33PT SC are shown in Figs. 2.2 and 2.3.

The orientation dependences of the electromechanical properties of the SC from the $3m$ symmetry class are characterised by the following important features [11].

1. Electromechanical constants Π'_{33} are independent of the Euler angle φ , where $\Pi = d, e, g, h, k, s^E$, and ε^σ .
2. There are two variants of periodicity on the Euler angle ψ . First, for Π'_{3j} with $j=1; 2$,

$$\Pi'_{31}(\varphi, \psi, \theta) = \Pi'_{32}(\varphi, \psi + 90^\circ, \theta) \text{ and } \Pi'_{32}(\varphi, \psi, \theta) = \Pi'_{31}(\varphi, \psi + 90^\circ, \theta), \quad (2.2)$$

and second,

$$\Pi'_{33}(\varphi, \psi, \theta) = \Pi'_{33}(\varphi, \psi + 90^\circ, \theta). \quad (2.3)$$

3. Periodicity on the Euler angle φ is a result of the presence of a three-fold axis in the $3m$ symmetry class [15]. As a consequence, the following equality holds:

$$\Pi'_{3j}(\varphi, \psi, \theta) = \Pi'_{3j}(\varphi + 120^\circ, \psi, \theta), \quad (2.4)$$

where $j = 1, 2$ and 3 .

4. The piezoelectric coefficients d'_{3j} show a periodical dependence as follows:
 - (i) at $\theta = 90^\circ$, independently of φ and ψ , the sum of the piezoelectric coefficients (i.e., the analogue of the hydrostatic piezoelectric coefficient d_h of the poled FC [14]) obeys a condition

$$d'_{31}(\varphi, \psi, 90^\circ) + d'_{32}(\varphi, \psi, 90^\circ) + d'_{33}(\varphi, \psi, 90^\circ) = 0, \quad (2.5)$$

- (ii) at $\varphi = 0$, $\psi = 45^\circ + 90^\circ p$ ($p = 1, 2$ and 3) and independently of θ , condition

$$d'_{31}(0, \psi, \theta) = d'_{32}(0, \psi, \theta) \quad (2.6)$$

is valid,

- (iii) at $\varphi > 0$, $\psi = 45^\circ + 90^\circ p$ ($p = 1, 2$ and 3) and $\theta = 90^\circ$, an equality

$$d'_{31}(\varphi, \psi, 90^\circ) = d'_{32}(\varphi, \psi, 90^\circ) \quad (2.7)$$

holds, and

- (iv) at $\varphi = 30^\circ + 60^\circ q$ ($q = 1, 2, 3, 4$, and 5), $\theta = 90^\circ$ and independently of ψ , condition

¹ It should be added that examples of the orientation dependence of ECFs k'_{ij} , thickness-mode ECF k'_t and planar-mode ECF k'_p for the single-domain KNbO₃ SC in the ferroelectric $mm2$ phase were discussed by Nakamura and Kawamura [13].

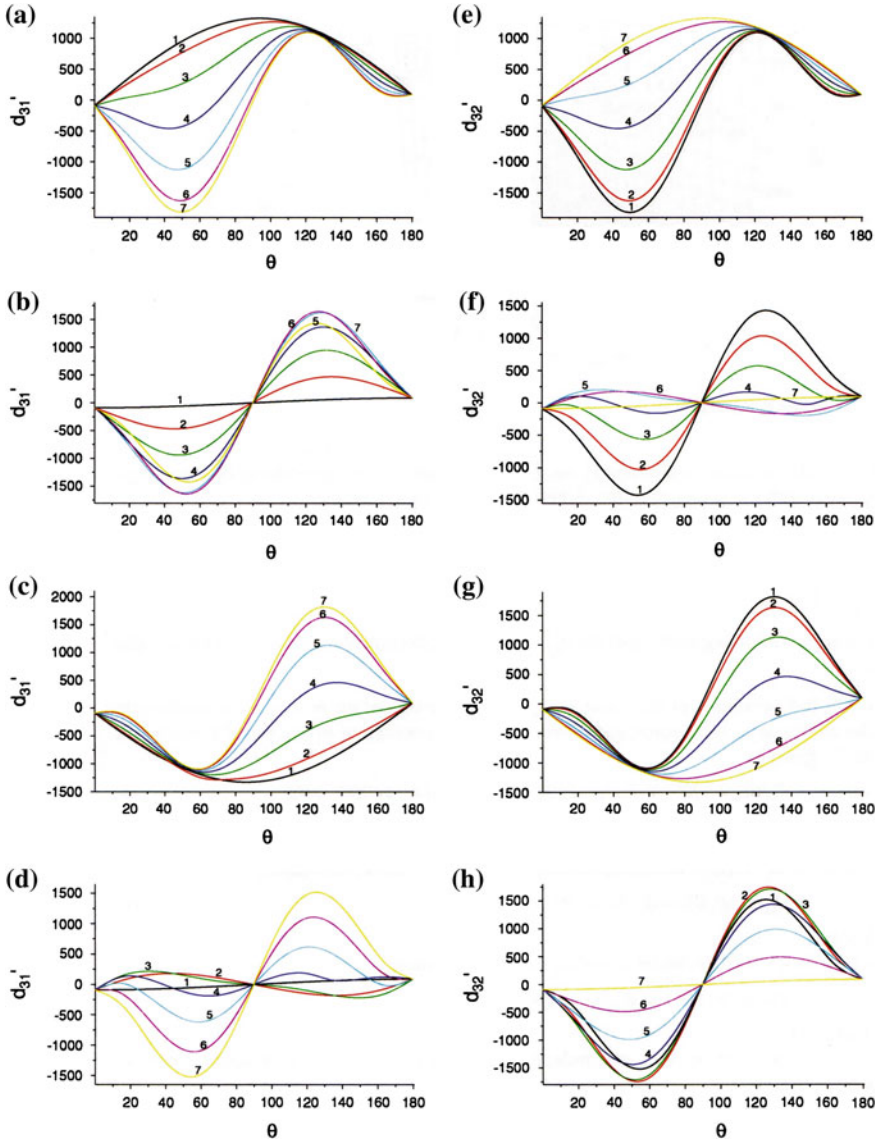


Fig. 2.2 Piezoelectric coefficients $d'_{3j}(\varphi, \psi, \theta)$ (d'_{3j} in pC/N, and φ, ψ and θ in degrees) calculated for the single-domain PMN–0.33PT SC: **a** $j = 1$ and $\varphi = 120^\circ p$, **b** $j = 1$ and $\varphi = 30^\circ + 120^\circ p$, **c** $j = 1$ and $\varphi = 60^\circ + 120^\circ p$, **d** $j = 1$ and $\varphi = 90^\circ + 120^\circ p$, **e** $j = 2$ and $\varphi = 120^\circ p$, **f** $j = 2$ and $\varphi = 30^\circ + 120^\circ p$, **g** $j = 2$ and $\varphi = 60^\circ + 120^\circ p$, **h** $j = 2$ and $\varphi = 90^\circ + 120^\circ p$, and **i** $j = 3$, no dependence on ψ . In graphs **a–h**, curves 1, 2, 3, 4, 5, 6, and 7 are related to $\psi = 0, 15, 30, 45, 60, 75$, and 90° , respectively, and $p = 0, 1, 2$, and 3 (reprinted from paper by Topolov [11], with permission from IOP Publishing)

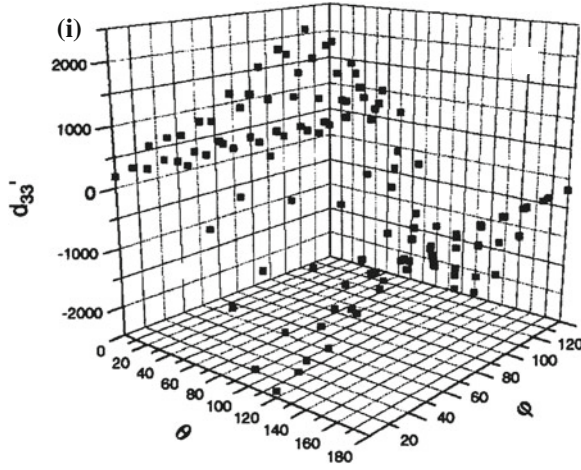


Fig. 2.2 (continued)

$$d'_{31}(\varphi, \psi, 90^\circ) = d'_{32}(\varphi, \psi, 90^\circ) = d'_{33}(\varphi, \psi, 90^\circ) = 0 \quad (2.8)$$

holds, i.e., no piezoelectric response is registered along the OX'_3 axis. Condition (2.8) can be regarded as a specific case of validity of condition (2.5).

An analysis of conditions (2.2)–(2.4) and (2.6)–(2.8) enables us to consider electromechanical constants Π'_{3j} of the single-domain PMN–0.33PT SC in the following ranges of the Euler angles:

$$0 \leq \varphi \leq 120^\circ, 0 \leq \psi \leq 90^\circ \text{ and } 0 \leq \theta \leq 180^\circ. \quad (2.9)$$

Equations (2.2)–(2.9) suggest that the periodicity of the orientation dependence $\Pi'_{3j}(\varphi, \psi, \theta)$ stems from features of the crystal structure of the $3m$ symmetry class [11] and should be taken into consideration in piezoelectric applications.

Comparing the curves in Figs. 2.2 and 2.3 at the corresponding fixed φ angles, one can conclude that the transformation of the curves $d'_{3j} \rightarrow k'_{3j}$ is mainly due to the influence of elastic compliances $s^{Ej}_{rt}(\varphi, \psi, \theta)$ of the single-domain SC. Dielectric permittivities $\varepsilon^{\sigma j}_{pq}(\varphi, \psi, \theta)$ influence the orientation dependence of ECFs $k'_{3j}(\varphi, \psi, \theta)$ to a lesser degree and may be due to the lower rank of the $\varepsilon^{\sigma}_{pq}$ tensor in comparison to the rank of the s^E_{rt} tensor. In general, the comparative analysis of graphs from Figs. 2.2 and 2.3 enable us to conclude that the anisotropy of d'_{3j} and k'_{3j} can be varied within specific ranges. These ranges mainly depend on the anisotropy of d_{3j} and s^E_{rt} which are related to the main crystallographic axes (see Table 2.1).

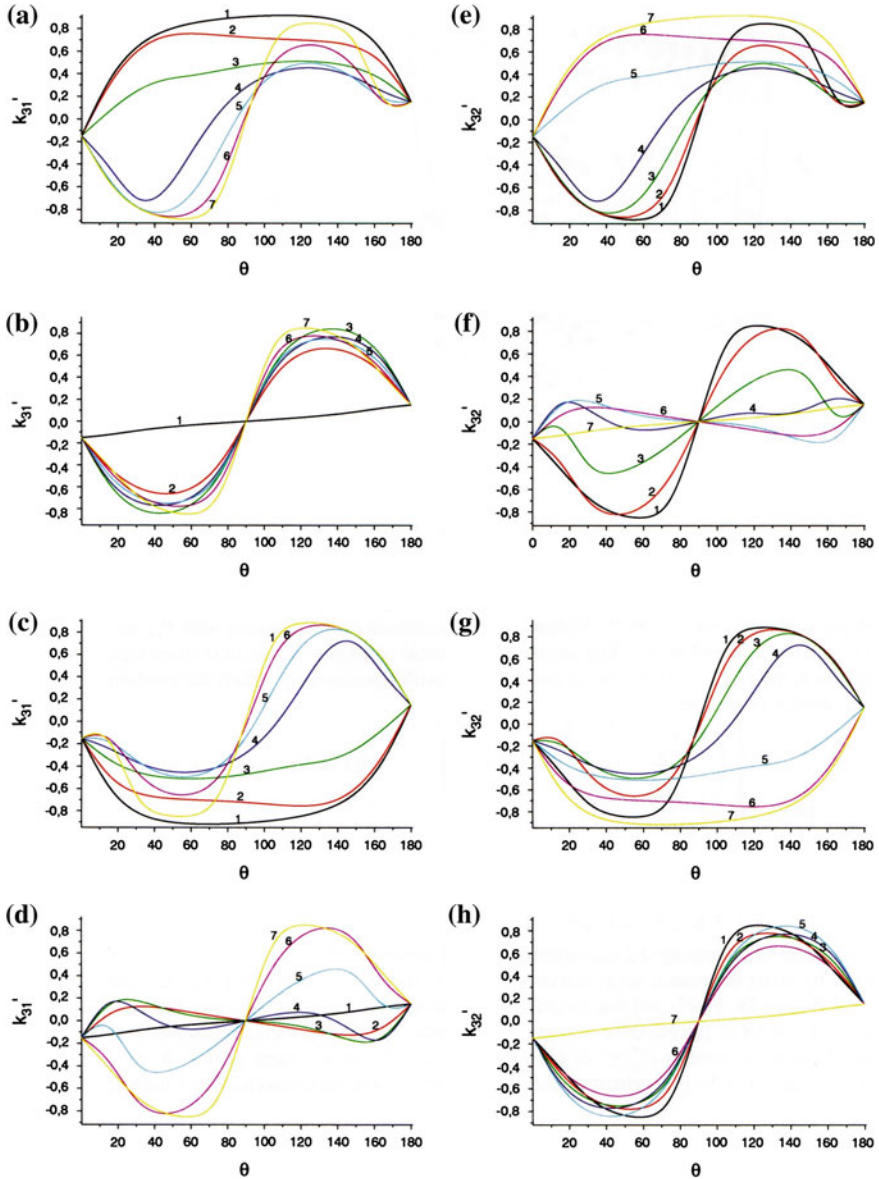


Fig. 2.3 ECFs $k'_{3j}(\varphi, \psi, \theta)$ (φ, ψ and θ in degrees) calculated for the single-domain PMN-0.33PT SC: **a** $j = 1$ and $\varphi = 120^\circ p$, **b** $j = 1$ and $\varphi = 30^\circ + 120^\circ p$, **c** $j = 1$ and $\varphi = 60^\circ + 120^\circ p$, **d** $j = 1$ and $\varphi = 90^\circ + 120^\circ p$, **e** $j = 2$ and $\varphi = 120^\circ p$, **f** $j = 2$ and $\varphi = 30^\circ + 120^\circ p$, **g** $j = 2$ and $\varphi = 60^\circ + 120^\circ p$, **h** $j = 2$ and $\varphi = 90^\circ + 120^\circ p$, and **i** $j = 3$, no dependence on ψ . In graphs **a-h**, curves 1, 2, 3, 4, 5, 6, and 7 are related to $\psi = 0, 15, 30, 45, 60, 75$, and 90° , respectively, and $p = 0, 1, 2$, and 3 (reprinted from paper by Topolov [11], with permission from IOP Publishing)

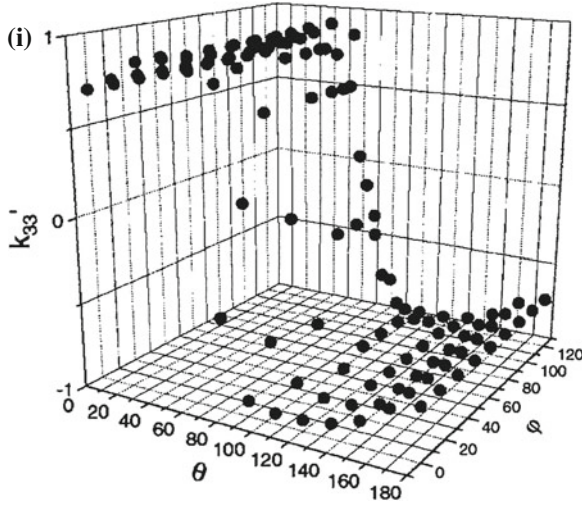


Fig. 2.3 (continued)

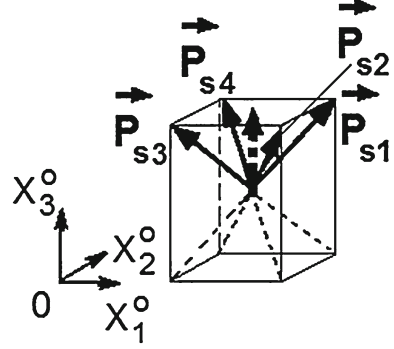
2.2 Polydomain $0.67\text{Pb}(\text{Mg}_{1/3}\text{Nb}_{2/3})\text{O}_3 - 0.33\text{PbTiO}_3$

Polydomain states (multidomains, domain-engineered states) are often formed in bulk relaxor-ferroelectric SC samples [1, 2] when the electric poling direction is not along the spontaneous polarisation vectors of the separate domain types. It is assumed that the $(001)_c$ cut of the rhombohedral PMN- x PT SC, poled along the $[001]_c$ perovskite unit-cell direction, is split into $71^\circ(109^\circ)$ domains that are mechanical twin components distributed regularly over the sample. Spontaneous polarisation vectors \mathbf{P}_{si} in these domains (Fig. 2.4) are given in the coordinate system $(X_1^\circ X_2^\circ X_3^\circ)$ by $\mathbf{P}_{s1}(P, P, P)$, $\mathbf{P}_{s2}(P, -P, P)$, $\mathbf{P}_{s3}(-P, -P, P)$, and $\mathbf{P}_{s4}(-P, P, P)$. The $71^\circ(109^\circ)$ domains are separated by the planar $\{100\}_c$ -type domain walls [1, 16, 17] that are permissible according to work [18, 19]. Based on the aforementioned domain arrangement, we consider two examples of the effective (average) electromechanical properties in polydomain PMN-0.33PT SCs.

2.2.1 Two Domain Types

We consider a laminar domain structure that is characterised by two domain types with $\mathbf{P}_{s1}(P, P, P)$ and $\mathbf{P}_{s2}(P, -P, P)$ (see the vector orientations in Fig. 2.4). These domains are regularly distributed over the SC sample and are separated by stress-free domain walls with normal vectors $\mathbf{n}_i \parallel [001]_c$. We assume that the volume fractions of the domains with \mathbf{P}_{s1} and \mathbf{P}_{s2} equal h and $1 - h$, respectively. The electromechanical

Fig. 2.4 Schematic of 71° (109°) domain types in the $[001]_c$ -poled rhombohedral SC. Axes of the co-ordinate system ($X_1^\circ X_2^\circ X_3^\circ$) are parallel to the crystallographic axes of the perovskite unit cell. The resulted (average) spontaneous polarisation vector (see the dotted arrow) is parallel to $O X_3^\circ || [001]_c$



propti of the i th domain type are determined in the ($X_1^\circ X_2^\circ X_3^\circ$) system in accordance with (2.1), and the rotation matrices are

$$\|r\| = \begin{pmatrix} 1/\sqrt{2} & -1/\sqrt{2} & 0 \\ 1/\sqrt{6} & 1/\sqrt{6} & -2/\sqrt{6} \\ 1/\sqrt{3} & 1/\sqrt{3} & 1/\sqrt{3} \end{pmatrix}$$

for $i = 1$ and

$$\|r\| = \begin{pmatrix} 1/\sqrt{2} & 0 & -1/\sqrt{2} \\ 1/\sqrt{6} & 2/\sqrt{6} & 1/\sqrt{6} \\ 1/\sqrt{3} & -1/\sqrt{3} & 1/\sqrt{3} \end{pmatrix}$$

for $i = 2$.

Averaging the electromechanical properties in this laminar domain structure is carried out using the matrix approach developed in works [14, 20–22]. A full set of the effective elastic compliances $s_{ri}^{E*}(h)$, piezoelectric coefficients $d_{fj}^*(h)$ and dielectric permittivities $\varepsilon_{pq}^{\sigma*}(h)$ of the polydomain SC is calculated [11] at $0 < h < 1$. We remind that the aforementioned effective properties in the polydomain state are determined in the long-wave approximation [14, 20] so that the wavelength of an external field is much longer than the thickness of the individual domains of the SC sample.

Based on the volume-fraction dependences of the effective electromechanical properties, ECFs $k_{3j}^*(h)$ and the remaining effective constants of the polydomain SC are determined. Minima of $|d_{3j}^*(h)|$ and $|k_{3j}^*(h)|$ are observed at $h = 0.5$, i.e., at equal volume fractions of the 71° (109°) domains. The largest values of $|d_{3j}^*(h)|$ and $|k_{3j}^*(h)|$ are related to single-domain states, i.e., $h = 0$ or $h = 1$. The same volume-fraction dependence [11] holds true for the laminar domain structure with \mathbf{P}_{s1} (volume fraction h) and \mathbf{P}_{s4} (volume fraction $1 - h$), while the spontaneous polarisation vector \mathbf{P}_s^* of the polydomain SC has only one component depending on h , and this

component is related to one of the non-poling directions, OX_1° or OX_2° . We note that the relatively low piezoelectric activity of the polydomain SC (spontaneous polarisation vectors \mathbf{P}_{s1} and \mathbf{P}_{s2} or \mathbf{P}_{s1} and \mathbf{P}_{s4}) is a result of the re-distribution of internal electric and mechanical stress fields [11] and may be associated with clamping of the non-180° domains in the presence of the domain walls with $\mathbf{n}_i || [001]_c$.

2.2.2 Four Domain Types

The next example of the effective electromechanical properties is related to the domain structure with four \mathbf{P}_{si} orientations (Fig. 2.4). Similar domain structures are often observed [2–4] in domain-engineered PMN-*x*PT and PZN-*x*PT SC samples poled along the OX_3° direction. To define the volume fractions v_i of the four domain types, we represent v_i in terms of two parameters, t and n , as follows:

$$v_1 = tn, v_2 = t(1 - n), v_3 = (1 - t)(1 - n), \quad \text{and} \quad v_4 = (1 - t)n \quad (2.10)$$

The effective electromechanical properties of the polydomain SC are calculated [11] on the basis of a two-step averaging procedure described in paper [23]. Graphs of $d_{3j}^*(t, n)$ and $k_{3j}^*(t, n)$, which characterise the piezoelectric activity and electro-mechanical coupling of the polydomain SC along the poling axis OX_3° , are shown in Fig. 2.5. As in the case of the two domain types (see Sect. 1.2.1), the present domain structure (Fig. 2.4) provides a decrease in both $|d_{3j}^*(t, n)|$ and $|k_{3j}^*(t, n)|$ at $t \rightarrow 0.5$ and/or $n \rightarrow 0.5$. A comparison of graphs of $d_{33}^*(t, n)$ (Fig. 2.5c) and $k_{33}^*(t, n)$ (Fig. 2.5d) enables us to conclude that elastic compliance $s_{33}^{E*}(t, n)$ and dielectric permittivity $\varepsilon_{33}^{\sigma*}(t, n)$ slightly influence ECF $k_{33}^*(t, n)$. As a consequence, the piezoelectric coefficient $d_{33}^*(t, n)$ plays a key role in forming this electromechanical coupling. However, $d_{33}^*(t, n)$ (Fig. 2.5c) decreases in a fairly narrow range which may be due to the orientation of the domain walls [11] in the polydomain state.

According to the room-temperature data [4] of PMN–0.33PT SC poled along the $[001]_c$ axis (4mm symmetry), experimental values of the piezoelectric coefficients are $d_{31,exp}^* = -1,330$ pC/N and $d_{33,exp}^* = 2,820$ pC/N. The macroscopic 4mm symmetry means that the four domain types shown in Fig. 2.4 would be present in the SC sample and volume fractions of these domain types are equal. The significant discrepancy between the calculated value of $d_{33}^*(0.5, 0.5) \approx 300$ pC/N (see Fig. 2.5c) and the above-given experimental $d_{33,exp}^*$ value is in good agreement with one of the conclusions of work [10] and could be due to the presence of an intermediate ferroelectric monoclinic phase [24, 25] near the MPB, by the non-180° domain coexistence [26] or by displacements of interfaces [24, 27] that separate two coexisting phases under the external electric field $\mathbf{E} || [001]_c$. Unfortunately, the lack of experimental data on the interconnections between the electromechanical properties of the single-domain and polydomain PMN-*x*PT SCs do not enable a comparison of the different results to any great degree. However some results of the present study are important for an

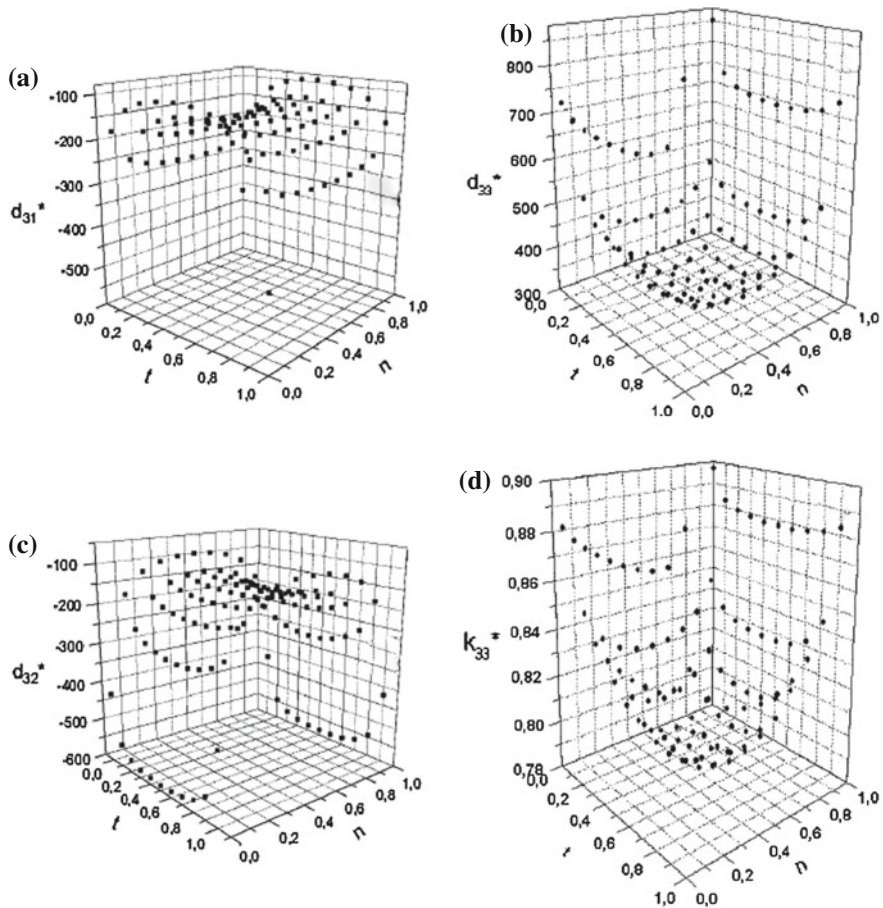


Fig. 2.5 Effective piezoelectric coefficients $d_{3j}^*(t, n)$ (in pC/N, graphs **a–c**) and ECF $k_{33}^*(t, n)$ (graph **d**) of the polydomain PMN-0.33PT SC (reprinted from paper by Topolov [11], with permission from IOP Publishing). The domain arrangement is shown in Fig. 2.4

interpretation of the complex links between the electromechanical properties in the SC and composite samples based on SCs that can be either polydomain or single-domain. Data on $d_{3j}^*(t, n)$ (Fig. 2.5a–c) are to be taken into account in the study of the anisotropy of the effective electromechanical properties of the composites based on SCs.

2.3 Single-Domain $(1-x)\text{Pb}(\text{Zn}_{1/3}\text{Nb}_{2/3})\text{O}_3 - x\text{PbTiO}_3$

Relaxor-ferroelectric PZN- x PT SCs are of great interest due to their various heterophase states [25, 28–31] and their outstanding electromechanical properties [16, 24, 26, 32] near the MPB ($x \approx 0.08\text{--}0.09$). The electromechanical constants of PZN- x PT SCs were determined for $0.045 \leq x \leq 0.12$ [3, 6, 33–37] on samples with engineered domain structures and in the single-domain state (Table 2.2). Electromechanical constants measured on single-domain SC samples are known, e.g., for PZN-0.09PT (intermediate monoclinic phase) and PZN-0.12PT (tetragonal $4mm$ phase). As is seen even for compositions away from the MPB, some discrepancies exist between the sets of electromechanical constants (see for instance, data for $x = 0.12$ in Table 2.2). These discrepancies can be accounted for by the poling conditions and heterogeneity of the SC samples.

The orientation dependences of the piezoelectric coefficients $d'_{3j}(\varphi, \psi, \theta)$ and $g'_{3j}(\varphi, \psi, \theta)$ and dielectric permittivity $\varepsilon'_{33}(\varphi, \psi, \theta)$ of single-domain monoclinic PZN-0.09PT SCs were analysed by Topolov [38]. Results from these orientation dependences were first systematised on the basis of a group of criteria and compared with known experimental data. Based on the criteria from work [38], the description of periodic and other changes in the piezoelectric and dielectric properties of a low-symmetry single-domain sample was carried out in terms of the Euler angles. Specific features of the dielectric anisotropy and high piezoelectric activity in the single-domain state were considered. The dielectric anisotropy (see data on ε'_{pp} at $x = 0.09$ from Table 2.2) influences the piezoelectric sensitivity of the single-domain PZN-0.09PT SC at various orientations of its crystallographic axes.

Table 2.2 Elastic compliances s_{ab}^E (in 10^{-12} Pa $^{-1}$), piezoelectric coefficients d_{ij} (in pC/N) and dielectric permittivities ε_{pp}^σ of single-domain PZN- x PT SCs

x	s_{11}^E	s_{12}^E	s_{13}^E	s_{33}^E	s_{44}^E	s_{66}^E	d_{31}
0.12 [33, 34]	20.1	−4.6	−18.2	54.5	19.5	17.2	−207
0.12 [36] ^a	22.4	−3.53	−20.95	58	—	27.86	−217
0.12 [35]	18.0	−0.185	−19.1	52.8	27.0	45.5	−130
0.09 [26] ^b	—	—	—	—	—	—	120
x	d_{32}	d_{33}	d_{15}	d_{24}	$\varepsilon'_{11}/\varepsilon_0$	$\varepsilon'_{22}/\varepsilon_0$	$\varepsilon'_{33}/\varepsilon_0$
0.12 [33, 34]	−207	541	653	653	10,000	10,000	750
0.12 [36] ^a	−217	576	—	—	—	—	870
0.12 [35]	−130	326	946	946	6,160	6,160	566
0.09 [26] ^b	−270	250	3,200	950	9,000	21,000	800

^a In work [36] electromechanical properties of the single-domain BiScO₃–PbTiO₃ SC are compared to the properties of the single-domain PZN-0.12PT SC, however no full set of electromechanical constants of PZN-0.12PT SC is present. The SCs of BiScO₃–PbTiO₃ and PZN-0.12PT are characterised by tetragonal symmetry

^b No full set of elastic constants of the single-domain PZN-0.09PT SC is known from literature data. To characterise the piezoelectric and dielectric properties of the monoclinic single-domain PZN-0.09PT SC, Dammak et al. [26] used the matrices that have forms [15] similar to those in the ferroelectric $mm2$ phase [39] of the single-domain KNbO₃ SC

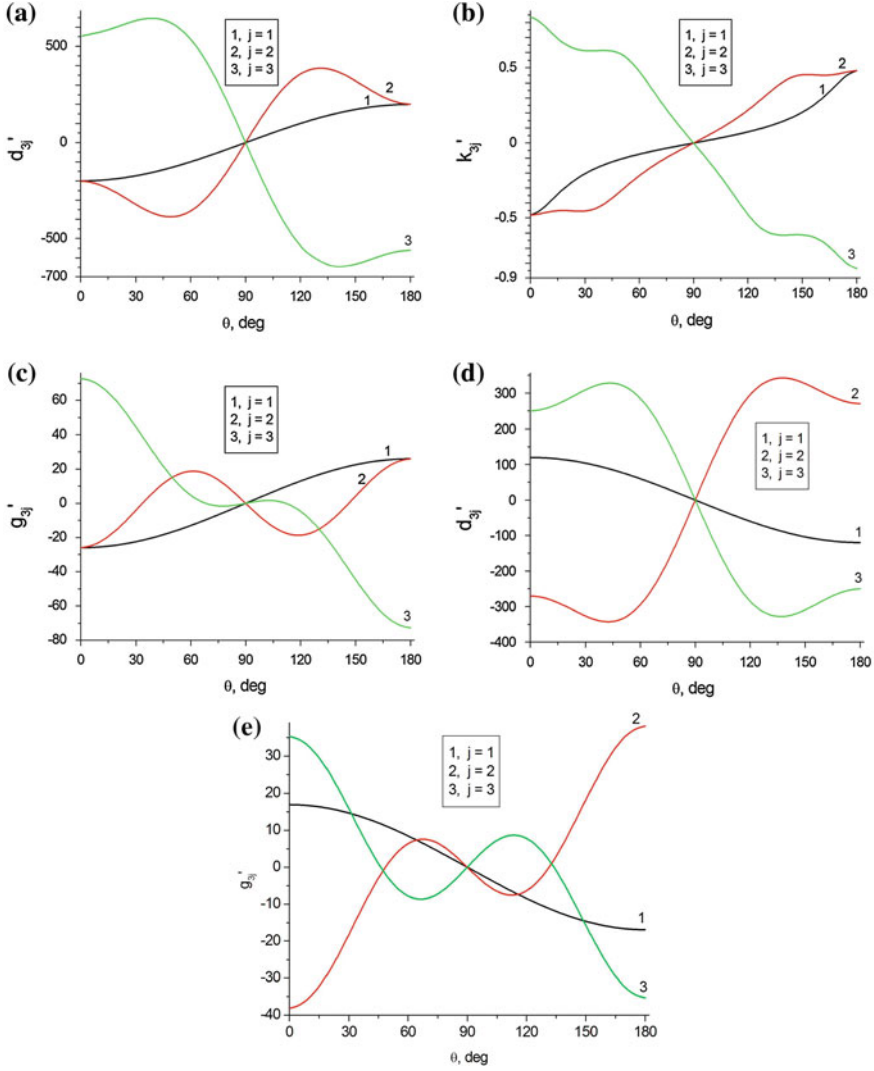


Fig. 2.6 Piezoelectric coefficients $d'_{3j}(\theta)$ (in pC/N, graphs **a** and **d**) and $g'_{3j}(\theta)$ (in mV·m / N, graphs **c** and **e**) and ECFs $k'_{3j}(\theta)$ (graph **b**) of single-domain PZN- x PT SCs at $\varphi = \psi = 0^\circ$: **a-c**, $x = 0.12$ and **d** and **e**, $x = 0.09$. Calculations for $x = 0.12$ and $x = 0.09$ were performed using data from [36] and [26], respectively (see Table 2.2)

As follows from work [11, 38], the electromechanical properties are represented by subscripts $i3$ and $3j$ and are highly dependent on the Euler angle θ (Fig. 2.1b) that directly links the spontaneous polarisation vector \mathbf{P}_s to the OX_3 axis. Taking into account the key role of the piezoelectric coefficients d_{3j} in various piezoelectric applications [13–16, 40–42], we consider examples of the orientation dependences

of the piezoelectric coefficients d'_{3j} and g'_{3j} and ECFs k'_{3j} on θ (Fig. 2.6). It should be noted that $\max d'_{33}(\theta)$ and $\min d'_{3j}(\theta)$ are achieved in both cases (Fig. 2.6a and d) irrespective of symmetry of SCs, and the condition $|d'_{33}(\theta)| > d'_{33}(0^\circ)$ is valid due to the effect of the large shear piezoelectric coefficients d_{15} and d_{24} (see Table 2.2). The distinctions between the curves of $g'_{3j}(\theta)$ related to $x = 0.12$ (Fig. 2.6c) and $x = 0.09$ (Fig. 2.6e) stem from the anisotropy of the piezoelectric coefficients d_{3j} and dielectric permittivities ε_{pp}^σ of the studied single-domain SCs.

Comparing the graphs of $d'_{3j}(\theta)$ to $g'_{3j}(\theta)$ (cf. Fig. 2.6a, c and Fig. 2.6d, e), one can observe an interesting feature of the orientation dependence of the piezoelectric response: the condition $\text{sgn } d'_{33}(\theta) = -\text{sgn } g'_{33}(\theta)$ holds in certain ranges of the Euler angle θ . Such a discrepancy of signs is due to the influence of dielectric permittivity $\varepsilon_{23}^{\sigma'}(\theta)$ on the piezoelectric coefficient $g'_{33}(\theta)$ [see for instance, Eqs. (1.12) and (1.14)]. This influence becomes considerable when $|\varepsilon_{23}^{\sigma'}| \sim \varepsilon_{pp}^{\sigma'}$ ($p = 1, 2$ and 3) and, therefore, an interconnection between $d'_{33}(\theta)$ and $g'_{33}(\theta)$ becomes more complicated, depending on the balance of some components of $\varepsilon_{pq}^{\sigma'}(\theta)$.

2.4 Single-Domain $x\text{Pb}(\text{In}_{1/2}\text{Nb}_{1/2})\text{O}_3 - y\text{Pb}(\text{Mg}_{1/3}\text{Nb}_{2/3})\text{O}_3 - (1-x-y)\text{PbTiO}_3$

The ternary system of relaxor-ferroelectric solid solutions of $x\text{Pb}(\text{In}_{1/2}\text{Nb}_{1/2})\text{O}_3 - y\text{Pb}(\text{Mg}_{1/3}\text{Nb}_{2/3})\text{O}_3 - (1-x-y)\text{PbTiO}_3$ (PIN- $x-y$) with a perovskite-type structure is of interest due to the considerable piezoelectric activity and anisotropy of the electromechanical properties. The full sets of electromechanical constants of the single-domain PIN- $x-y$ SCs have been measured at room temperature (Table 2.3). Despite the relatively small difference in the composition, these SCs are related to different symmetry classes ($3m$ for PIN-0.24–0.49 [43], $mm2$ for PIN-0.27–0.40 [44] and $4mm$ for PIN- $x-y$, without the definitive chemical composition [45]) and show clear distinctions in the anisotropy of the electromechanical properties. It should be added that the PIN-0.24–0.49 SCs maintain the single-domain state without an electric bias field [43].

The very large piezoelectric coefficients d_{15} and d_{24} (approximately 11.7–13 times more than the longitudinal piezoelectric coefficient d_{33}) in the single-domain PIN-0.27–0.40 SC are of value to study the effect of the orientation of crystallographic axes on the piezoelectric performance and related parameters. The coercive field E_c of PIN- $x-y$ SC is on the order of 10 kV/cm [45] which is a few times higher than E_c of the neighbouring rhombohedral compositions and tetragonal PMN- x PT SCs [46]. The strong shear-mode piezoelectric effect and electromechanical coupling in the single-domain PIN- $x-y$ SC [45] along with the large E_c value is of interest for piezo-technical applications such as actuators and transducers which are exploited in a relatively wide range of electric fields E .

Examples of the orientation dependences (Fig. 2.7) suggest that a similarity between the $d'_{3j}(\theta)$ and $k'_{3j}(\theta)$ curves is observed for the single-domain PIN- $x-y$ SCs from various symmetry classes. Such orientation behaviour is accounted for by

Table 2.3 Room-temperature elastic compliances s_{ab}^E (in 10^{-12} Pa $^{-1}$), piezoelectric coefficients d_{ij} (in pC/N) and dielectric permittivities ε_{pp}^σ of single-domain PIN-0.24–0.49 [43], PIN-0.27–0.40 [44] and PIN- x - y [45] SCs

Composition	s_{11}^E	s_{12}^E	s_{13}^E	s_{14}^E	s_{23}^E	s_{23}^E	s_{33}^E	s_{44}^E
PIN-0.24–0.49	11.62	−7.81	−1.10	22.17	11.62	−1.10	6.05	93.33
PIN-0.27–0.40	9.20	−8.38	5.64	0	21.2	−14.4	16.8	78.1
PIN- x - y	17.1	−3.3	−14.2	0	17.1	−14.2	41	55.0
Composition	s_{55}^E	s_{66}^E	d_{15}	d_{22}	d_{24}	d_{31}	d_{32}	d_{33}
PIN-0.24–0.49	93.33	38.86	2,015	−490	2,015	−21	−21	75
PIN-0.27–0.40	316	15.5	4,550	0	4,100	153	−346	350
PIN- x - y	55.0	25.0	2,350	0	2,350	−200	−200	530
Composition	$\frac{\varepsilon_{11}^\sigma}{\varepsilon_0}$	$\frac{\varepsilon_{22}^\sigma}{\varepsilon_0}$	$\frac{\varepsilon_{33}^\sigma}{\varepsilon_0}$					
PIN-0.24–0.49	5,800	5,800	650					
PIN-0.27–0.40	8,070	30,000	1,500					
PIN- x - y	15,000	15,000	1,090					

the leading role of the piezoelectric properties and their anisotropy in forming the orientation dependence of ECF $k'_{3j}(\theta)$ (Fig. 2.7b, d and f). The role of symmetry of the relaxor-ferroelectric SCs is also to be taken into account by interpretation of the orientation effects and the anisotropy of d'_{3j} , k'_{3j} etc. Moreover, lowering the symmetry gives rise to a more complex link between the $d'_{3j}(\theta)$ and $k'_{3j}(\theta)$ curves (see for instance, Fig. 2.7a and b). This link is predominantly concerned with the anisotropy of the elastic and dielectric properties in the low-symmetry phases. As in Fig. 2.6, max $d'_{33}(\theta)$ and min $d'_{3j}(\theta)$ are achieved (Fig. 2.7a, c and e) irrespective of the symmetry class and is a result of the strong shear piezoelectric effect ($d_{15} > d_{33}$, see Table 2.3).

2.5 Conclusion

In this chapter important examples of the orientation dependences of the piezoelectric coefficients and ECFs are considered for ferroelectric-relaxor SCs in the single-domain state. Volume-fraction dependences of the piezoelectric properties are analysed for the polydomain relaxor-ferroelectric SCs. The non-monotonic orientation dependences of the piezoelectric coefficients d'_{3j} and g'_{3j} and ECFs k'_{3j} are analysed in terms of the Euler angles φ , ψ and θ .

Variants of periodicity of the electromechanical properties are explained by taking into consideration unit-cell symmetry elements. The role of the shear piezoelectric effect due to the large piezoelectric coefficients d_{15} and d_{24} is discussed in the context of the non-monotonic orientation dependence of d'_{3j} .

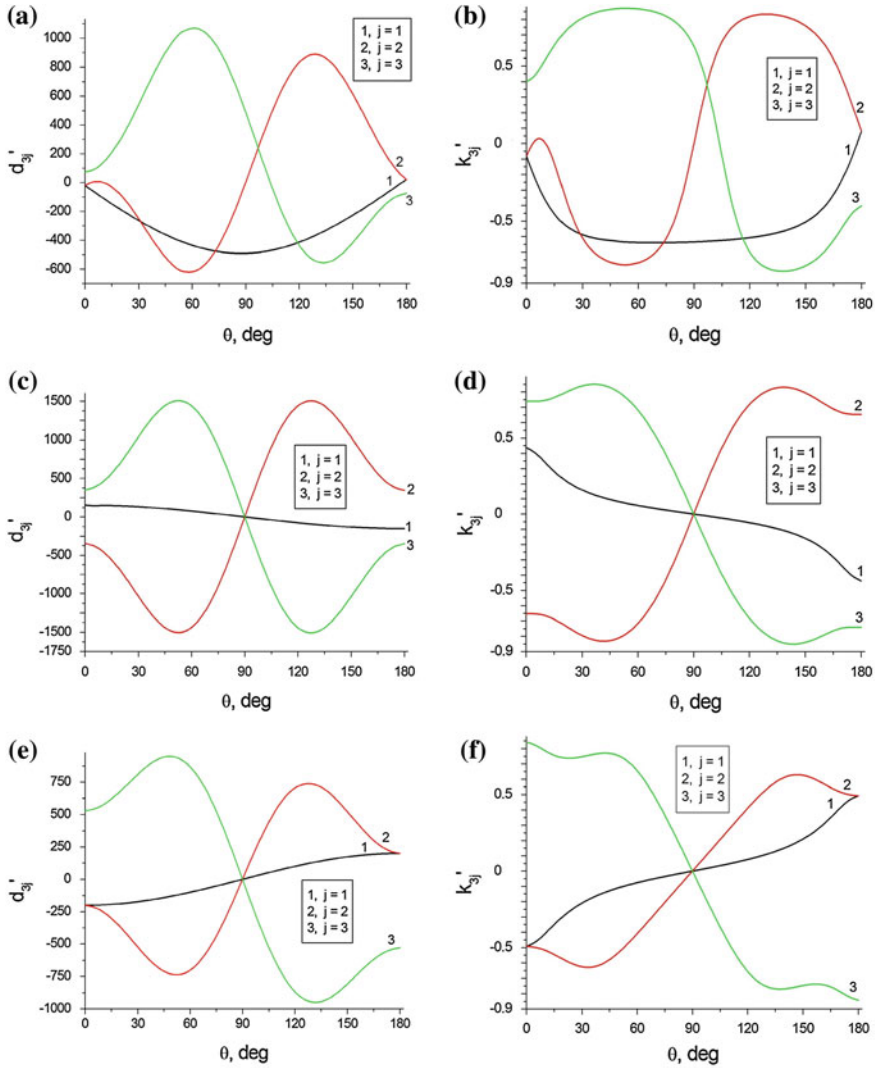


Fig. 2.7 Piezoelectric coefficients $d'_{3j}(\theta)$ (in pC/N, graphs **a**, **c** and **e**) and ECFs $k'_{3j}(\theta)$ (graphs **b**, **d** and **f**) of single-domain PIN-0.24-0.49 (**a** and **b**), PIN-0.27-0.40 (**c** and **d**) and PIN- x - y (**e** and **f**) SCs at $\varphi = \psi = 0^\circ$. Calculations were performed using data from Table 2.3

Two examples of the effect of a 71° (109°) domain structure on the electro-mechanical properties are considered in the $3m$ phase of the PMN-0.33PT SC. This SC in the polydomain state (with either two or four domain types) is characterised by $\min |d_{3j}^*|$ and $\min |k_{3j}^*|$ in the “most symmetrical” cases of the domain arrangement, i.e., for equal volume fractions of the 71° (109°) domains separated by the planar $\{100\}_c$ -type walls and the domain-wall displacement is neglected over the SC sample. In this context we deal with the so-called intrinsic contribution of the

non-180° domain structures on the effective electromechanical properties of SCs. Of course, the influence of an additional (extrinsic) contribution from the domain-wall and interphase-boundary displacements on the electromechanical properties would be needed and may be a subject of further studies.

Results shown in Figs. 2.2, 2.3, 2.6, and 2.7 suggest that the anisotropy of the piezoelectric coefficients d'_{3j} and ECFs k'_{3j} can be varied in a relatively wide range due to the orientation effect. This variation is achieved even by changing one of the Euler angles, for instance, θ (see the θ angle in Fig. 2.1b).

Undoubtedly, the role of symmetry is important in the interpretation of the orientation dependences of the electromechanical properties and their anisotropy in relaxor-ferroelectric SCs. Irrespective of the symmetry class, the electromechanical properties represented by subscripts $i3$ and $3j$ are highly dependent on the Euler angle θ that directly links the spontaneous polarisation vector \mathbf{P}_s of the SC to the co-ordinate OX_3 axis (see Fig. 2.1). Taking into account features of the orientation behaviour of the piezoelectric coefficients d'_{3j} , one can analyse the remaining groups of the piezoelectric coefficients (e'_{3j} , g'_{3j} and h'_{3j}), ECFs k'_{3j} and related parameters which are of interest for sensor, actuator, transducer, and other applications.

References

1. Wada S, Park S-E, Cross LE, Shrout TR (1999) Engineered domain configuration in rhombohedral PZN-PT single crystals and their ferroelectric related properties. *Ferroelectrics* 221:147–155
2. Yin J, Cao W (2000) Domain configurations in domain engineered 0.955Pb(Zn_{1/3}Nb_{2/3})O₃-0.045PbTiO₃ single crystals. *J Appl Phys* 87:7438–7441
3. Yin J, Cao W (2002) Effective macroscopic symmetries and materials properties of multidomain 0.955Pb(Zn_{1/3}Nb_{2/3})O₃-0.045PbTiO₃ single crystals. *J Appl Phys* 92:444–448
4. Zhang R, Jiang B, Cao W (2001) Elastic, piezoelectric, and dielectric properties of multidomain 0.67Pb(Mg_{1/3}Nb_{2/3})O₃-0.33PbTiO₃ single crystals. *J Appl Phys* 90:3471–3475
5. Zhang R, Jiang W, Jiang B, Cao W (2002) Elastic, dielectric and piezoelectric coefficients of domain engineered 0.70Pb(Mg_{1/3}Nb_{2/3})O₃-0.30PbTiO₃ single crystal. In: Cohen RE (ed) *Physics of ferroelectrics*. American Institute of Physics, Melville, pp 188–197
6. Zhang R, Jiang B, Cao W, Amin A (2002) Complete set of material constants of 0.93Pb(Zn_{1/3}Nb_{2/3})O₃-0.07PbTiO₃ domain engineered single crystal. *J Mater Sci Lett* 21:1877–1879
7. Zhang R, Jiang B, Cao W (2003) Single-domain properties of 0.67Pb(Mg_{1/3}Nb_{2/3})O₃-0.33PbTiO₃ single crystals under electric field bias. *Appl Phys Lett* 82:787–789
8. Noheda B (2002) Structure and high-piezoelectricity in lead oxide solid solutions. *Curr Opin Solid State Mater Sci* 6:27–34
9. Zhang R, Jiang B, Cao W (2003) Orientation dependence of piezoelectric properties of single domain 0.67Pb(Mn_{1/3}Nb_{2/3})O₃-0.33PbTiO₃ crystals. *Appl Phys Lett* 82:3737–3739
10. Damjanovic D, Budimir M, Davis M, Setter N (2003) Monodomain versus polydomain piezoelectric response of 0.67Pb(Mg_{1/3}Nb_{2/3})O₃-0.33PbTiO₃ single crystals along nonpolar directions. *Appl Phys Lett* 83:527–529; Erratum *ibid.* 2490
11. Topolov VYu (2004) The remarkable orientation and concentration dependences of the electromechanical properties of 0.67Pb(Mg_{1/3}Nb_{2/3})O₃-0.33PbTiO₃ single crystals. *J Phys: Condens Matter* 16:2115–2128

12. Ikeda T (1990) Fundamentals of piezoelectricity. Oxford University Press, Oxford, New York, Toronto
13. Nakamura K, Kawamura Y (2000) Orientation dependence of electromechanical coupling factors in KNbO_3 . IEEE Trans Ultrason Ferroelectr Freq Control 47:750–755
14. Topolov VYu, Bowen CR (2009) Electromechanical properties in composites based on ferroelectrics. Springer, London
15. Zheludev IS (1971) Physics of crystalline dielectrics, vol. 2. Electrical properties, Plenum, New York
16. Park S-E, Shrout TR (1997) Ultrahigh strain and piezoelectric behavior in relaxor based ferroelectric single crystals. J Appl Phys 82:1804–1811
17. Erhart J, Cao W (1999) Effective material properties in twinned ferroelectric crystals. J Appl Phys 86:1073–1081
18. Fousek J, Janovec V (1969) The orientation of domain walls in twinned ferroelectric crystals. J Appl Phys 40:135–142
19. Tagantsev AK, Cross LE, Fousek J (2010) Domains in ferroic crystals and thin films. Springer, New York
20. Akcakaya E, Farnell GW (1988) Effective elastic and piezoelectric constants of superlattices. J Appl Phys 64:4469–4473
21. Topolov VYu (1995) Anisotropy of electromechanical properties in KNbO_3 crystals with S-type domain boundaries. J Phys Condens Matter 7:7405–7408
22. Emelyanov AS, Raevskaya SI, Savenko FI, Topolov VYu, Raevski IP, Turik AV, Kholkin AL (2007) Dielectric and piezoelectric properties of (001)-oriented $(1 - x)\text{Pb}(\text{Mg}_{1/3}\text{Nb}_{2/3})\text{O}_3 - x\text{PbTiO}_3$ single crystals with $0.1 \leq x \leq 0.4$. Solid State Commun 143:188–192
23. Glushanin SV, Topolov VYu (2001) Features of electromechanical properties of piezoelectric composites with elements of connectivity 1–1. J Phys D Appl Phys 34:2518–2529
24. Topolov VYu, Turik AV (2002) An intermediate monoclinic phase and electromechanical interactions in $x\text{PbTiO}_3 - (1 - x)\text{Pb}(\text{Zn}_{1/3}\text{Nb}_{2/3})\text{O}_3$ crystals. Phys Solid State 44:1355–1362
25. Topolov VYu (2012) Heterogeneous ferroelectric solid solutions. Phases and domain states. Springer, Berlin
26. Dammak H, Renault A-É, Gaucher P, Thi MP, Calvarin G (2003) Origin of the giant piezoelectric properties in the [001] domain engineered relaxor single crystals. Jpn J Appl Phys, Pt 1 42:6477–6482
27. Topolov VYu, Turik AV (2001) Interphase boundaries and high piezoelectric activity of $x\text{PbTiO}_3 - (1 - x)\text{Pb}(\text{Zn}_{1/3}\text{Nb}_{2/3})\text{O}_3$ crystals. Phys Solid State 43:1117–1123
28. Fujishiro K, Vlokh R, Uesu Y, Yamada Y, Kiat J-M, Dkhil B, Yamashita Y (1998) Optical observation of heterophases and domain structure in relaxor ferroelectrics $\text{Pb}(\text{Zn}_{1/3}\text{Nb}_{2/3})\text{O}_3 / 9\% \text{PbTiO}_3$. Jpn J Appl Phys Part 1 37:5246–5248
29. Ye Z-G, Dong M, Zhang L (1999) Domain structure and phase transitions in relaxor-based piezo-/ferroelectric $(1 - x)\text{Pb}(\text{Zn}_{1/3}\text{Nb}_{2/3})\text{O}_3 - x\text{PbTiO}_3$ single crystals. Ferroelectrics 229:223–232
30. Topolov VYu, Ye Z-G (2001) Elastic matching of morphotropic phases in polydomain $(1 - x)\text{Pb}(\text{Zn}_{1/3}\text{Nb}_{2/3})\text{O}_3 - x\text{PbTiO}_3$ single crystals. Ferroelectrics 253:71–78
31. Topolov VYu (2003) Heterophase states in $0.10\text{PbTiO}_3 - 0.90\text{Pb}(\text{Zn}_{1/3}\text{Nb}_{2/3})\text{O}_3$ crystals. Phys Solid State 45:1295–1297
32. Ogawa T, Yamauchi Y, Numamoto Y, Matsushita M, Tachi Y (2002) Giant electromechanical coupling factor of k_{31} mode and piezoelectric d_{31} constant in $\text{Pb}[(\text{Zn}_{1/3}\text{Nb}_{2/3})_{0.91}\text{Ti}_{0.09}]\text{O}_3$ piezoelectric single crystal. Jpn J Appl Phys, Part 2 41:L55–L57
33. Guennou M, Dammak H, Thi MP (2008) 2 T domain-engineered piezoelectric single crystals: calculations and application to PZN-12%PT poled along [101]. J Appl Phys 104:074102 (6 pp.)
34. Guennou M (2007) Modifications des propriétés structurales et électromécaniques de monocristaux piézoélectriques $\text{Pb}(\text{Zn}_{1/3}\text{Nb}_{2/3})_{1-x}\text{Ti}_x\text{O}_3$: ingénierie des domaines et dopage au manganèse. Dr Thesis, École Centrale Paris, Châtenay-Malabry

35. Delaunay T (2006) Caractérisation fonctionnelle et relations structure - propriétés de monocristaux piézoélectriques de type pérovskite. Ph.D Thesis, Université François Rabelais de Tours, Tours
36. Zhang S, Randall CA, Shrout TR (2004) Dielectric, piezoelectric and elastic properties of tetragonal $\text{BiScO}_3\text{-PbTiO}_3$ single crystal with single domain. *Solid State Commun* 131:41–45
37. He C, Jing W, Wang F, Zhu K, Qui J (2011) Full tensorial elastic, piezoelectric, and dielectric properties characterization of [011]-poled PZN-9%PT single crystal. *IEEE Trans Ultrason Ferroelectr Freq Control* 58:1127–1130
38. Topolov VYu (2005) Orientation relationships between electromechanical properties of monoclinic $0.91\text{Pb}(\text{Zn}_{1/3}\text{Nb}_{2/3})\text{O}_3\text{-}0.09\text{PbTiO}_3$ single crystals. *Sens Actuat A* 121:148–155
39. Wiesendanger E (1974) Dielectric, mechanical and optical properties of orthorhombic KNbO_3 . *Ferroelectrics* 6:263–281
40. Uchino K (1997) Piezoelectric actuators and ultrasonic motors. Kluwer, Boston
41. Gorish AV, Dudkevich VP, Kupriyanov MF, Panich AE, Turik AV (1999) Piezoelectric device-making, vol. 1. Physics of ferroelectric ceramics. Radiotekhnika, Moscow (in Russian)
42. Haertling G (1999) Ferroelectric ceramics: history and technology. *J Am Ceram Soc* 82:797–818
43. Sun E, Cao W, Jiang W, Han P (2011) Complete set of material properties of single domain $0.24\text{Pb}(\text{In}_{1/2}\text{Nb}_{1/2})\text{O}_3\text{-}0.49\text{Pb}(\text{Mg}_{1/3}\text{Nb}_{2/3})\text{O}_3\text{-}0.27\text{PbTiO}_3$ single crystal and the orientation effects. *Appl Phys Lett* 99:032901 (3 pp.)
44. Zhang S, Liu G, Jiang W, Luo J, Cao W, Shrout TR (2011) Characterization of single domain $\text{Pb}(\text{In}_{0.5}\text{Nb}_{0.5})\text{O}_3\text{-Pb}(\text{Mg}_{1/3}\text{Nb}_{2/3})\text{O}_3\text{-PbTiO}_3$ crystals with monoclinic phase. *J Appl Phys* 110:064108 (5 pp.)
45. Li F, Zhang S, Xu Z, Wei X, Luo J, Shrout TR (2010) Electromechanical properties of tetragonal $\text{Pb}(\text{In}_{1/2}\text{Nb}_{1/2})\text{O}_3\text{-Pb}(\text{Mg}_{1/3}\text{Nb}_{2/3})\text{O}_3\text{-PbTiO}_3$ ferroelectric crystals. *J Appl Phys* 107:054107 (5 pp.)
46. Cao H, Schmidt VH, Zhang R, Cao W, Luo H (2004) Elastic, piezoelectric, and dielectric properties of $0.58\text{Pb}(\text{Mg}_{1/3}\text{Nb}_{2/3})\text{O}_3\text{-}0.42\text{PbTiO}_3$ single crystal. *J Appl Phys* 96:549–554

Piezo-Active Composites

Orientation Effects and Anisotropy Factors

Topolov, V.Y.; Bisegna, P.; Bowen, C.R.

2014, XV, 169 p. 48 illus., 31 illus. in color., Hardcover

ISBN: 978-3-642-38353-3